Liquid Crystals
Publication details, including instructions for authors and subscription information:
http://www.informaworld.com/smpp/title~content=t713926090

Thermal and current-voltage behaviour of liquid crystal compounds with rod and bent shapes comprising alkoxysemifluorinated and imine segments

Agnieszka Iwan[a]; Henryk Janeczek[b]; Agnieszka Hreniak[a]; Marcin Palewicz[ac]; Damian Pociecha[d]
[a] Electrotechnical Institute, Division of Electrotechnology and Materials Science, Wroclaw, Poland [b] Centre of Polymer and Carbon Materials, Polish Academy of Sciences, Zabrze, Poland [c] Institute of Electrical Engineering Fundamentals, Wroclaw University of Technology, Wroclaw, Poland [d] University of Warsaw, Department of Chemistry, Warsaw, Poland

Online publication date: 16 August 2010

To cite this Article Iwan, Agnieszka , Janeczek, Henryk , Hreniak, Agnieszka , Palewicz, Marcin and Pociecha, Damian(2010) 'Thermal and current-voltage behaviour of liquid crystal compounds with rod and bent shapes comprising alkoxysemifluorinated and imine segments', Liquid Crystals, 37: 8, 1021 — 1031
To link to this Article: DOI: 10.1080/02678291003746262
URL: http://dx.doi.org/10.1080/02678291003746262

Liquid Crystals,
Vol. 37, No. 8, August 2010, 1021–1031

Taylor & Francis
Taylor & Francis Group

Thermal and current–voltage behaviour of liquid crystal compounds with rod and bent shapes comprising alkoxysemifluorinated and imine segments

Agnieszka Iwan[a]*, Henryk Janeczek[b], Agnieszka Hreniak[a], Marcin Palewicz[a,c] and Damian Pociecha[d]

[a]*Electrotechnical Institute, Division of Electrotechnology and Materials Science, M. Sklodowskiej-Curie 55/61 Street, 50-369 Wroclaw, Poland;* [b]*Centre of Polymer and Carbon Materials, Polish Academy of Sciences, 34 M. Curie-Sklodowska Street, 41-819 Zabrze, Poland;* [c]*Institute of Electrical Engineering Fundamentals, Wroclaw University of Technology, 27 Wybrzeze Wyspianskiego Street, 50-370 Wroclaw, Poland;* [d]*University of Warsaw, Department of Chemistry, Zwirki i Wigury 101, 02-089 Warsaw, Poland*

(*Received 23 September 2009, final version received 3 March 2010*)

The synthesis and mesomorphic properties of a series of thermotropic liquid crystalline symmetrical rod and bent-shaped imines containing two long alkoxysemifluorinated chains were reported. Three different diamines varying in the number of phenylene rings from 1 to 3 were used to understand structure–mesomorphic property correlation. Differential scanning calorimetry, X-ray diffraction and polarised optical microscopy were used to determine their phase transition behaviour. An enantiotropic smectic phase was observed for all the systems studied. The thermal properties of the azomethines were discussed in relation to the core shape and length of the core. Current–voltage measurements were performed on ITO/compound/Alq_3/Al and ITO/TiO_2/compound/Alq_3/Al devices before and after irradiation with light (about 1000 W m^{-2}). To prepare the TiO_2 layer, the sol-gel technique was applied.

Keywords: imines; azomethines; Schiff bases; mesomorphic behaviour; fluorine compounds; bent-shaped and rod-like compounds

1. Introduction

Liquid crystal (LC) compounds exist between solid and liquid states and are highly structured liquids with orientational and/or positional orders of constituent molecules. The type of molecular order (nematic, cholesteric, smectic) is controlled by shape and chirality of LC molecules, and their molecular order is sensitive to temperature (thermotropic LC), electric and magnetic fields, or adsorption of chemicals (lyotropic LC). In recent years LC materials have received huge attention due to their optical properties and applications both in our daily life (cell phones, laptop displays, digital watches, calculators, etc.) and scientific optical applications (tunable waveguides, digital holography, optical processors, diffraction gratings, optical tweezers etc.). Among the large group of rod-like (calamitic) and disc-like (discotic mesogens) LC compounds, many researchers have investigated the influence of fluoric substituents or chain fluorination on the liquid crystalline properties of various classes of mesogens, such as oligomers [1, 3–14], discotic LC [1, 15–20], supramolecular LC [1, 21–22] and lyotropic LC and biological systems [1, 23–28]. Also, imines (often called azomethines or Schiff bases) with bent [29–33] and rod shapes [34–51] are the subject of investigation as mesogenic materials. Liquid crystalline azomethines can be divided into rod-shaped imines and bent-shaped (also referred to as banana-shaped) imines. Moreover, LC imines have been investigated concerning the symmetry of the molecule, and can be divided into unsymmetrical and symmetrical imines. Unsymmetrical imines with fluorinated chains were investigated by Bilgin-Eran *et al.* [39] and Iwan *et al.* [51]. Bilgin-Eran *et al.* [39] found that the thermal behaviour of the fluorinated imines depends on the number of chains, the substitution pattern and the number of fluorine atoms in the fluoricoalkyl chains. Through increasing the number of F atoms in the fluoricoalkyl chains, stabilisation of smectic and columnar mesophases was observed [39]. We recently reported the synthesis, characterisation and mesomorphic properties of unsymmetrical imines based on 4-(4,4,5,5,6,6,7,7,8,8,9,9,10,10,11,11,11-heptadecafluoroundecyloxy)benzaldehyde [51]. Enantiotropic smectic phases were observed for all the systems studied. We did not find papers concerning LC properties of symmetrical imines with rod and bent shapes comprising two alkoxysemifluorinated chains.

Why did we selected imines with semifluorinated chains as an object for study? First, fluorine substitution is an effective tool used to influence the electronic properties of semiconducting compounds such as oligothiophenes [39, 52–53]. Second, fluoric substituents are important for the design of LC materials [1, 39]. For example, F substitution of the aromatic core changed such properties as LC phase transition

*Corresponding author. Email: a.iwan@iel.wroc.pl

ISSN 0267-8292 print/ISSN 1366-5855 online

DOI: 10.1080/02678291003746262
http://www.informaworld.com

temperatures, dielectric properties, birefringence and elastic constants [1, 39]. Fluoric substituents at terminal chains caused completely different effects [1, 39]. The incorporation of a fluorinated chain into the compound enhances the thermal stability of the LC mesophases and modifies the mesophase morphologies in comparison with the same compound with aliphatic chains.

The studies reported here were devoted to a few symmetrical rod and bent-shaped imines with a long alkoxysemifluorinated chain (-O-$(CH_2)_3$-$(CF_2)_7$-CF_3) with different core. Additionally, a bent-shaped azomethine derived from 4-octadecyloxybenzaldehyde was synthesised and its properties compared with others. The LC properties were investigated by differential scanning calorimetry (DSC) and polarising optical microscopy (POM). Current–voltage measurements were performed on ITO/compound/Alq_3/Al and ITO/TiO_2/compound/Alq_3/Al devices. To prepare the TiO_2 layer the sol-gel technique was applied. To the best of our knowledge, the mesomorphic properties of the symmetrical rod and bent-shaped imines with semifluorinated chain have been not investigated so far.

With this background it is important to know the influence of structural parameters on the specific properties of the compounds.

2. Results and discussion

2.1 Synthesis and characterisation

The imines described in this paper were prepared from 4-(4,4,5,5,6,6,7,7,8,8,9,9,10,10,11,11,11-heptadecafluoroundecyloxy)benzaldehyde and four aromatic amines via high temperature solution condensation in N,N-dimethylacetamide (DMA) at 160°C. In addition, an imine from diaminodiphenyl methane and 4-octadecyloxybenzaldehyde (**5**) was synthesised via high temperature solution condensation in DMA at 160°C. The chemical route along with the structures of the imines (abbreviated hereinafter as **1–5**) are presented in Figure 1, whereas details of the synthesis procedures for the imines are given in the Experimental details.

Their expected chemical constitution is confirmed by spectroscopic studies. In proton nuclear magnetic resonance (NMR) spectra of the investigated compounds, the azomethine proton signal was observed in the range of 8.38–8.45 ppm, as expected. In ^{13}C NMR spectra of all azomethines with a signal in the range of 160–161 ppm was detected, which confirmed the existence of a carbon atom in azomethine group (HC=N-). The presence of the imine group was also confirmed by Fourier transform infrared (FTIR) spectroscopy, since in each case the band characteristic of the HC=N- stretching deformations was detected. The exact position of this band varies in the spectral range 1622–1626 cm^{-1} (see Experimental details). In accordance with the NMR and FTIR data collected in the Experimental section, the spectral data obtained are in agreement with data predicted from the chemical formulae of the synthesised compounds.

Imines **1**, **2** and **4** were soluble with difficulty in chloroform, while azomethine **3** was insoluble in this solvent. Only the compound with two long aliphatic chains, that is, compound **5**, was easily soluble in chloroform solution. This behaviour clearly confirmed the influence of the chemical structure of the compounds on their solubility. Purity of all imines was confirmed by elemental analysis. Elemental analysis showed quite good agreement with the calculated values, and found content of carbon, nitrogen and hydrogen in the compounds (see Experimental details).

2.2 Current–voltage measurement

Devices with the architecture ITO/compound/Alq_3/Al and ITO/TiO_2/compound/Alq_3/Al were constructed and investigated before and after irradiation with light (halogen lamp, about 1000 W m^{-2}). Alq_3 plays the role of an electron injection transport and emitting layer.

Current–voltage (*I–V*) measurements of compounds **1**, **4** and **5** were carried out. From the obtained results it was possible to calculate a luminal voltage for illuminated and dark measurements. Differences between illuminated and not-illuminated devices were observed. It can be seen that for all the devices under illumination, current rapidly increases with applied voltage increase. The current–voltage curves of such devices as ITO/compound/Alq_3/Al and ITO/TiO_2/compound/Alq_3/Al before and after irradiation are shown in Figure 2.

For example, the turn-on voltage of the device ITO/**1**/Alq_3/Al was observed at about 7 V at room temperature under 1000 W m^{-2}, while for the device without illumination this was about 9 V. The turn-on voltage of the device ITO/TiO_2/**1**/Alq_3/Al under illumination of 1000 W m^{-2} was observed at about 3 V at room temperature, while for the same device without illumination the turn-on voltage was found at about 7 V.

Differences were found along with change of the compound's structure. It was observed that for ITO/**4**/Alq_3/Al the turn-on voltage was at about 10 V at room temperature without illumination, while for the device ITO/**4**/Alq_3/Al under 1000 W m^{-2} this was at about 7 V. The turn-on voltage of the device ITO/TiO_2/**4**/Alq_3/Al under illumination of 1000 W m^{-2} was observed at about 5 V at room temperature, while

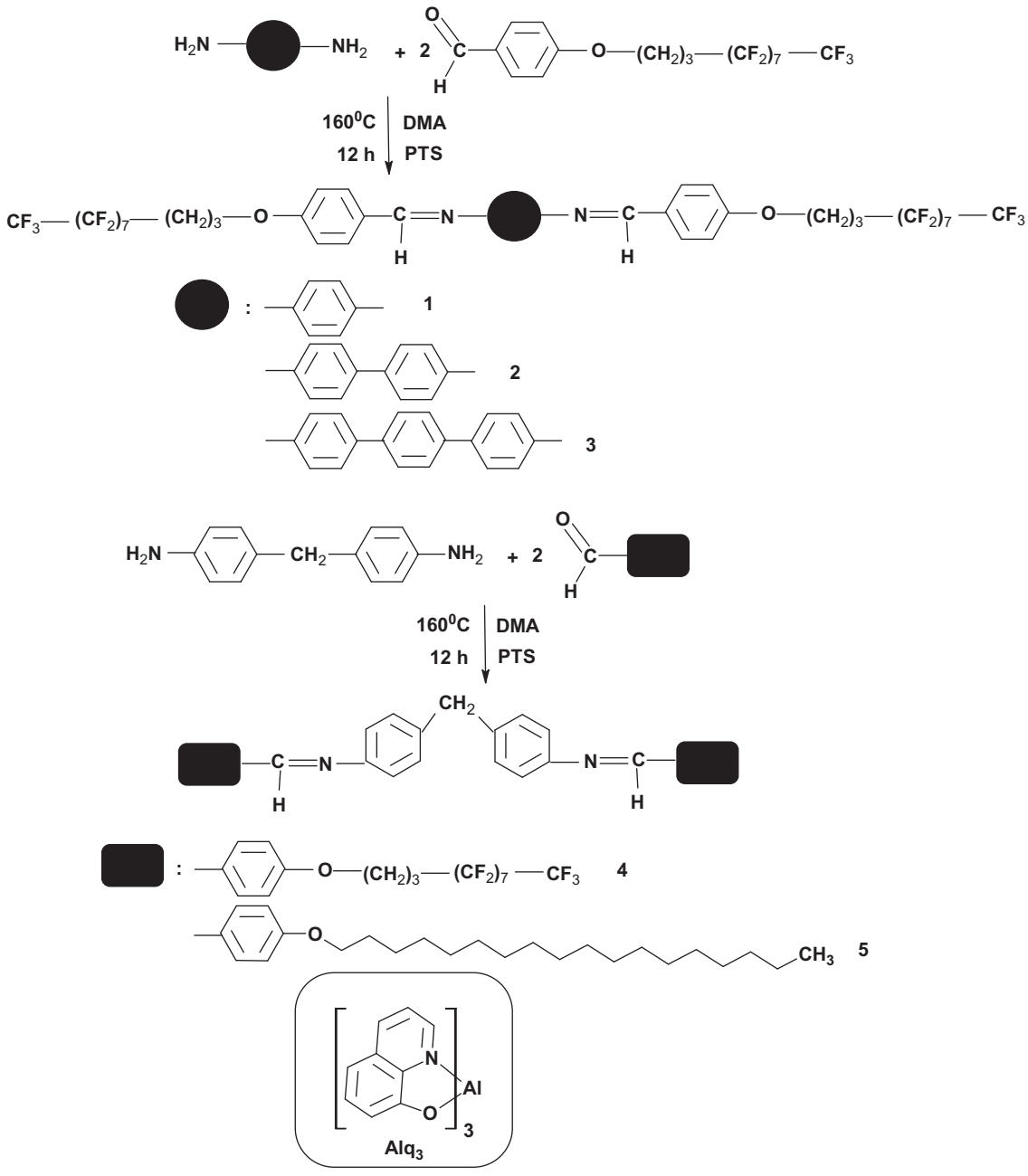

Figure 1. Synthetic route of the imines with the rod and bent shape and chemical structure of Alq_3.

for the same device without illumination it was found at about 6 V (Figure 2).

The turn-on voltage of the device ITO/**5**/Alq_3/Al was observed at about 5 V at room temperature without illumination and at 3 V under 1000 W m^{-2}. For the device ITO/TiO_2/**5**/Alq_3/ under illumination of 1000 W/m^2 the turn-on voltage was observed at about 6 V at room temperature, while for the same device without illumination it was found to be at about 9 V (Figure 2). This behaviour confirmed the influence of the compound structure on the *I–V* characteristic of the azomethines. The differences found in the *I–V* characteristics of the azomethines confirm the difference in planarity of the compound structures and the different conformations of the compound in film.

The conductivity value of the investigated compounds was about 10^{-8}–10^{-7} S m^{-1}, which categorises probe materials between semiconductors and dielectrics [30, 54–56]. The first conjugated polymer used for fabrication of an organic light emitting diode (OLED) was poly(p-phenylene vinylene) (PPV) with the device configuration ITO/PPV/Al, for which a substantial

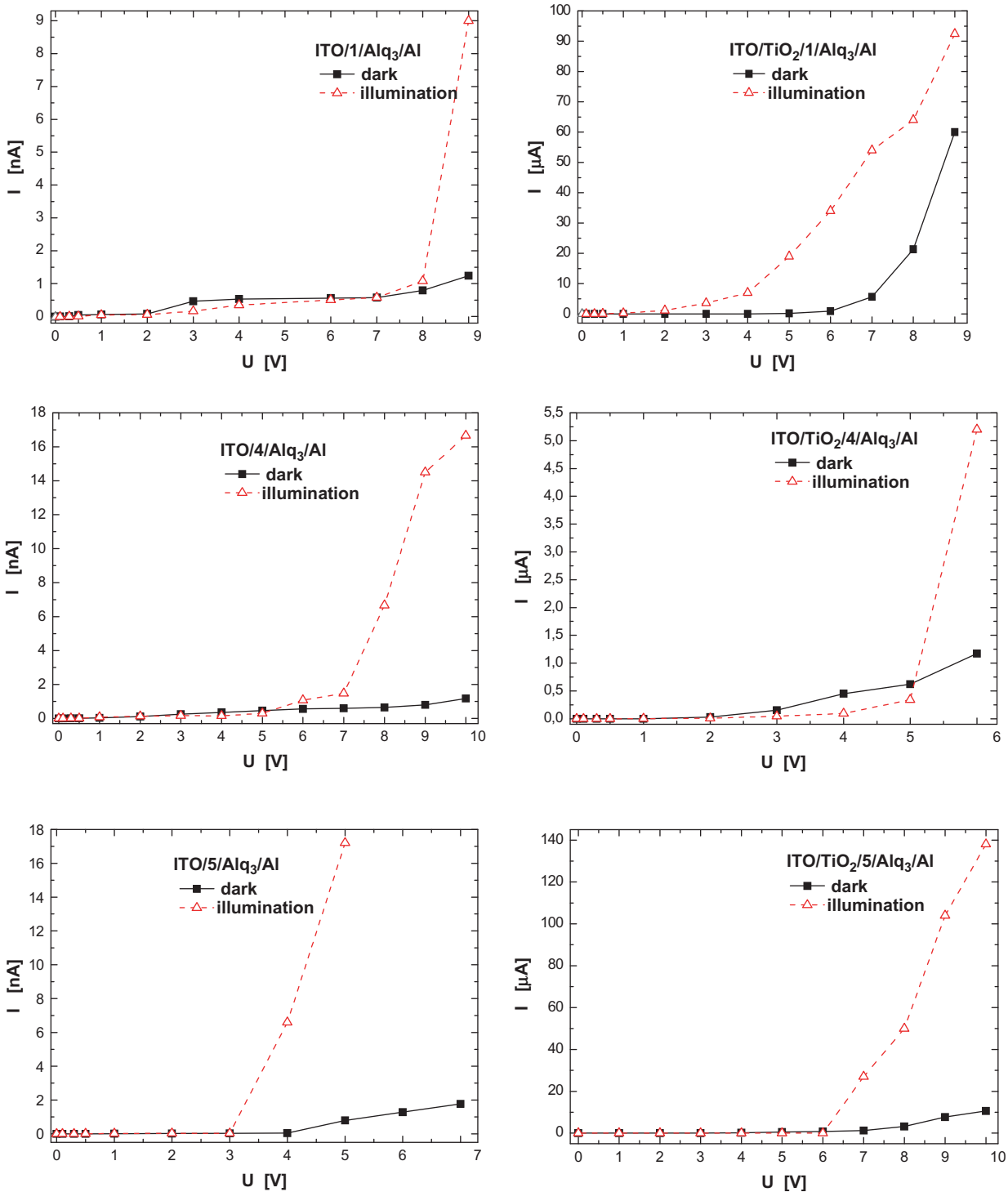

Figure 2. Current–voltage curves of ITO/compound/Alq_3/Al and ITO/TiO_2/compound/Alq_3/Al devices before and after irradiation with light.

charge injection was observed just below 14 V [57, 58]. The turn-on voltage of the devices ITO/PAZ-TPA/Alq_3/Al was observed at about 6 V [59]. We found no significant differences between *I–V* characteristic of our azomethines and polyazomethines with triphenylamine core (PAZ-TPA) in the main chain.

The conducted measurements indicate that significant photo-generation of charges (electrons)

occurred for devices with and without a TiO_2 layer. There were also significant increases in current from nano to micro amperes for devices with a TiO_2 layer.

Two different types of sample architecture were prepared to demonstrate that the connection of organic and inorganic compound improves the photo-electrical properties of devices which can be used as solar cells or OLEDs. We fabricated a series of OLED devices with an Alq_3 green-emitting layer serving as a reference OLED, and OLEDs with an additional hole transporting layer (HTL) consisting of a thin film of compound inserted between the ITO anode and the Alq_3 green-emitting layer. Our study suggests a potential new application of azomethines with rod and bent shapes by exploiting their hole (or electron) transport properties, paving the way toward stable organic optoelectronic devices (for example, OLEDs and solar cells) using azomethine based-HTLs, emissive layers, and electron transporting layers (ETLs).

2.3 Thermotropic behaviour

Several liquid crystal phases were observed by DSC and their nature was determined using X-ray and POM. The tentative mesophase identifications and the sequence of phase transitions related to all the compounds are based on the identification of textures appearing in two reference textbooks for liquid crystals [60, 61] and on repeated X-ray, POM and DSC experiments.

Figure 3 shows the DSC thermograms of the imines **1–4**, while the transition temperatures (T) and the transition enthalpies (ΔH) of the imines **1–5** determined by DSC along with the phase variants determined by POM are presented in Table 1.

From the DSC experiment, we note that most of the transition temperatures (T) increase with the length of the core (compare compounds **1–3**). On the other hand, compounds with the bent-shaped core (**4**) induced a decrease of the transition temperatures in comparison with the imine with rod shape (**2**) (Table 1). Similar behaviour was observed with changing

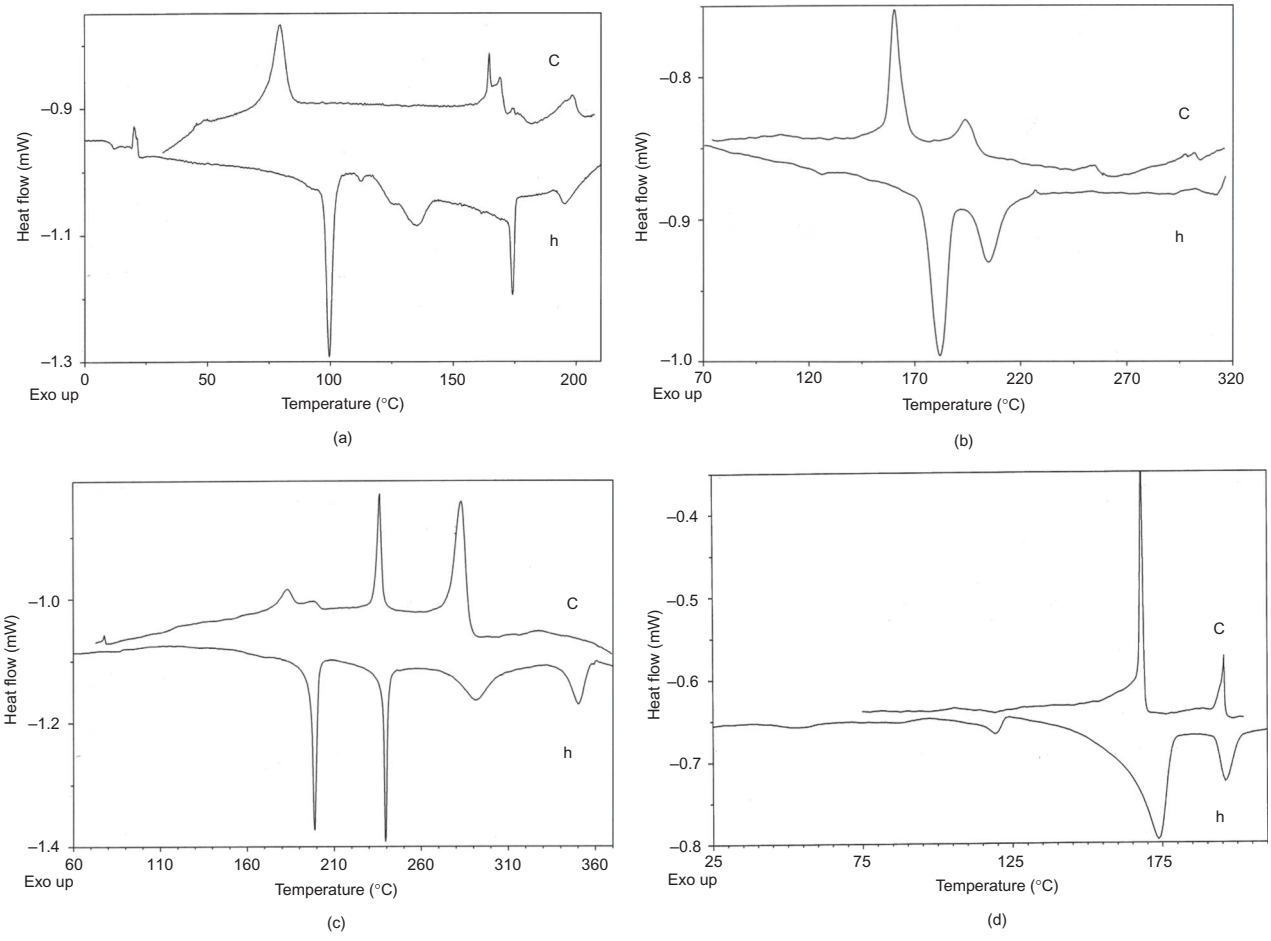

Figure 3. Differential scanning calorimetry traces of the: (a) **1**, (b) **2** (c) **3** and (d) **4** obtained on the second heating (h) and cooling (c), under N_2 atmosphere.

Table 1. Transition temperatures T (°C) and enthalpy changes ΔH (J g^{-1}) (in parentheses).

	DSC	POM
Code	T*(ΔH)	T
1	79 (2.6), 165 (1.4), 198 (0.8)	Cr < 70, SmA 185, I 206
2	160 (5.2), 193 (1.9), 255 (0.5), 302 (0.7)	Cr 193, SmC 250, I 313
3	183, 198 (3.6), 238 (2.2), 283 (5.5), 328 (1.9)	Cr 187, SmF 245, SmC 273, I > 350
4	106 (0.8), 168 (16.2), 196 (4.1)	Cr 118, SmA 171, I 201
5	42, 53 (11.8), 124 (64)	Cr 126

Note: * Cooling at 2°min^{-1}, $T \pm 0.1$°C, $\Delta H \pm 0.1$ J g^{-1}

alkoxysemifluorinated chains for the octadecyloxy one (compare compounds **4** and **5**).

Table 1 reveals that compounds **2** and **3** exhibited a clearing point temperature higher than 300°C, while compounds **1** and **4** have a clearing point temperature about 200°C. For the investigated imines different mesomorphic properties were observed (see Table 1). It is worth noting that, in accordance with the results of the DSC measurements, the clearing temperature distinctly increased in the following order: 124°C (**5**) < 197°C (**4**) < 205°C (**1**) < 302°C (**2**) < 328°C (**3**) upon the cooling cycle. This behaviour indicates the role of the mesogenic core structure in creating their mesomorphic properties. It should be noted that the phase transition temperature values seen in the DSC thermograms were almost equivalent to those of the transition temperatures estimated from POM investigations.

For the imine **1**, the typical black areas of a homeotropically aligned SmA mesophase (Figure 4(a)) with a few defects were observed [60, 61]. When we softly pressed the sample during cooling from its isotropic state, we occasionally saw the formation of some batonnet-like and small fan-like textures separating from a black background.

For the imine **2**, during cooling scans from 312°C to 193°C and heating scans from 193°C to 312°C, the development of the typical Schlieren texture of its SmC mesophase was repeatedly observed (Figure 4(b)) [60, 61]. The appearance of the homeotropically aligned texture of the SmC mesophase of **2** can be rationalised by the strong repulsion existing between the (apolar) alkoxysemifluorinated tails of this calamitic LC and the polar surface of the glass substrates.

Unfortunately, at a temperature close to clearing point (i.e. 310°C) of compound **2** we did not manage to capture a POM image of the SmC mesophase under planar alignment because of the evaporation the compound. Additionally, due to the temperature range accessible (from –196°C to 350°C) with hot stage used in our POM set-up, we have not been able to observed a full isotropisation of **2**.

During cooling in scans of **3** we observed a smooth (and difficult to unambiguously determine) SmF (or I) > Frozen SmF (SmI) transition at temperatures of around 187°C. In addition, for the compound **3** a SmC phase was detected (Figure 4(c)).On further cooling below 245°C (and to 187°C), we have observed the very slow formation of a paramorphotic (from the previously existing hometropically aligned SmC mesophase) coloured mosaic texture [60, 61]. The very fine lines defining the borders between mosaic domains and the absence of a typical Schlieren texture is in favour of its attribution to a highly ordered smectic F (or I) mesophase (Figure 4(d)) [60, 61].

For the bent-shaped imine **4** SmA phase was found along with (i) the planar (focal conic fan) texture (Figure 4(e)), (ii) the oriented (by soft mechanical shearing) planar texture, (iii) the homeotropically aligned texture (under soft pressure onto the sample) of a perfectly self-organised SmA monodomain, and (iv) the hometropically aligned texture combined with some typical SmA-like defects as well as the batonnet textures (Figure 4(f)) [60, 61].

For the bent-shaped imine **5** under POM investigation, only the crystallisation temperature and melting point are in good agreement with the exotherm (at around 122°C) and endotherm (at around 126°C) obtained by the DSC method.

The phase transitions were additionally analysed based on their enthalpy values (see Table 1). The melting process has the highest enthalpy values. The parameters of the heating and cooling process are similar. The phase transition with the smallest enthalpy values (0.7 J g^{-1}) was observed for compound **2** (see Table 1).

It should be mentioned that LC compounds which exhibit a mesophase or a sequence of mesophases over a broad and narrow temperature range could be used in: (i) colour information technology-based applications and (ii) organic electronic devices (OLEDs, organic solar cells).

In addition, the thermotropic behaviour of the investigated compounds was confirmed by small angle X-ray diffraction (SAXRD) and wide angle X-ray diffraction (WAXRD). All the mesogenic compounds form liquid-like smectic phases, either orthogonal smectic A phase (compounds **1** and **4**) or tilted smectic C phase (compounds **2** and **3**). The X-ray pattern of these phases is characterised by a sharp Bragg-type signal at low angle, corresponding to

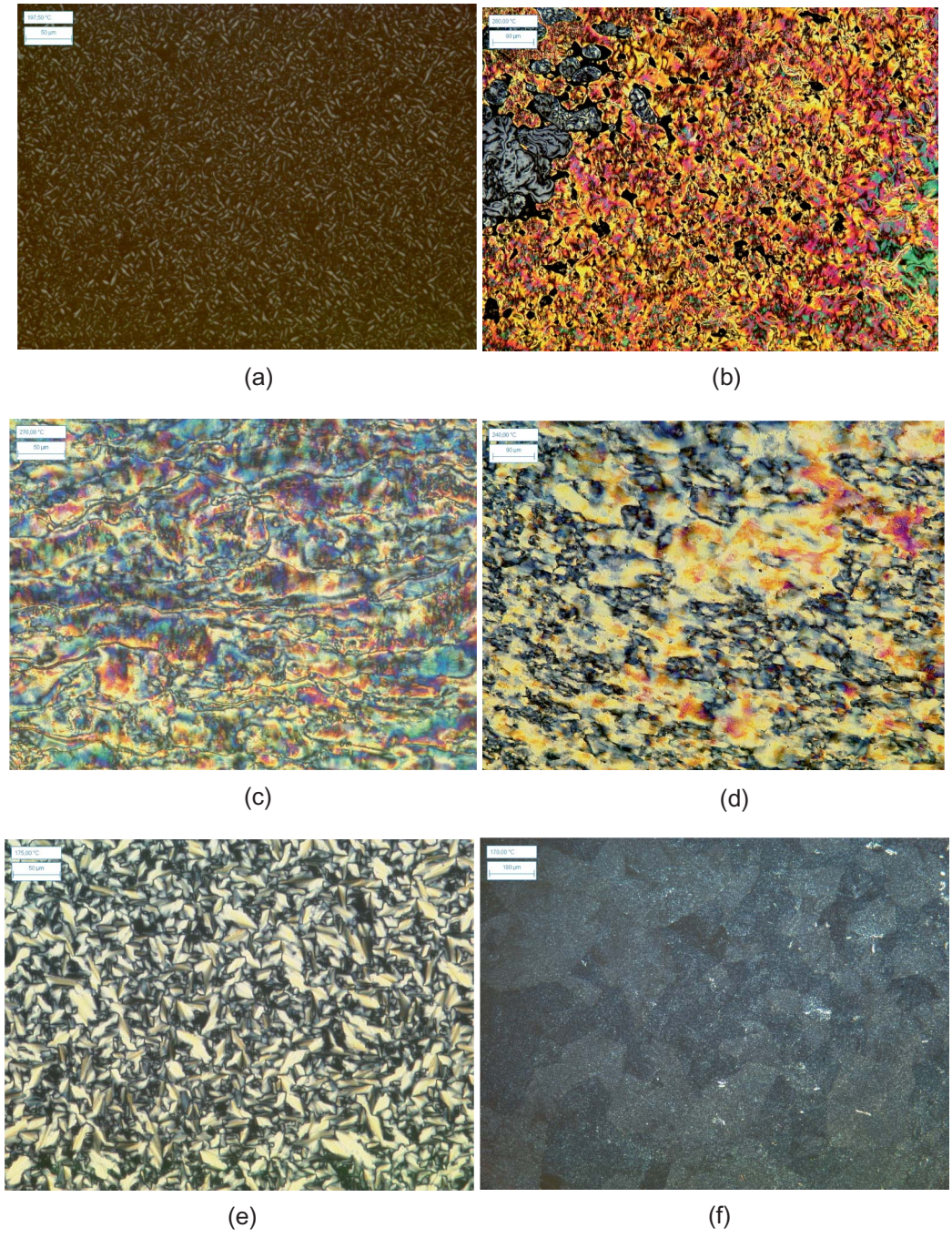

Figure 4. Photomicrographs of the optical textures of mesophases obtained for the: (a) **1:** SmA–batonet and small focal conic fan, (seen at 197.50°C), (b) **2**: Schliren texture, (seen at 280.00°C), (c) **3**: SmC-marble and sand-like textures, (seen at 270.00°C), (d) **3**: SmF-mosaic texture, (seen at 240.00°C), (e) SmA-Focal conic fan texture, (seen at 175.00°C) and (f) SmA-homeotropically aligned area and specific defects and SmA batonet textures, (seen at 196.80°C).

layer periodicity, and a broad diffused signal at high angle, related to short-range intermolecular positional correlations within layers (Figure 5). Compound **3** also forms hexatic SmF phase, in which long-range orientational order of local crystallographic axes direction appears. Onset of SmF phase manifests on the X-ray pattern as narrowing of the highest angle signal, reflecting growing correlation length of in-layer molecular ordering (Figure 5).

Figure 6 presents the behaviour of layer spacing in the cases of orthogonal and tilted smectic phases of compounds **4** and **2**, respectively. Decrease of layer

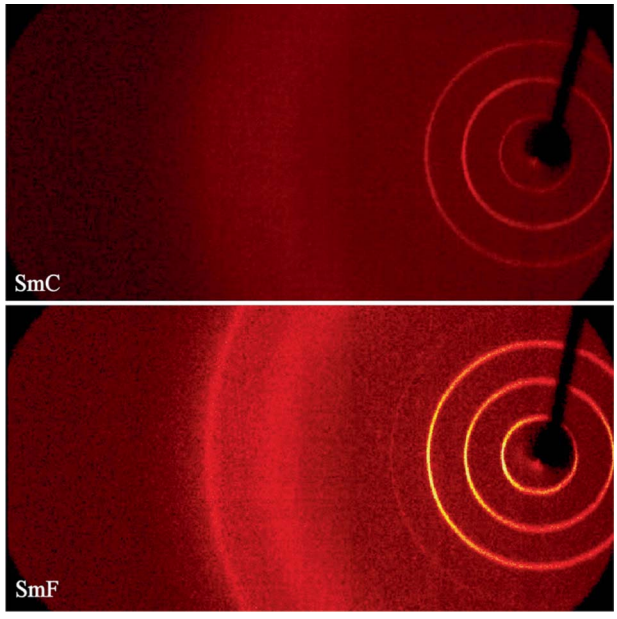

Figure 5. Wide angle X-ray patterns of SmC and SmF phases of compound **3**. Sharp low angle signals reflect layer periodicity, broad high angle signal comes from in-plane molecular position correlations. Two maxima in the high angle region appear because of partially fluorinated terminal chains. Narrowing of the most outer ring comes from increase of correlation length in hexatic SmF phase with respect to liquid-like SmC phase.

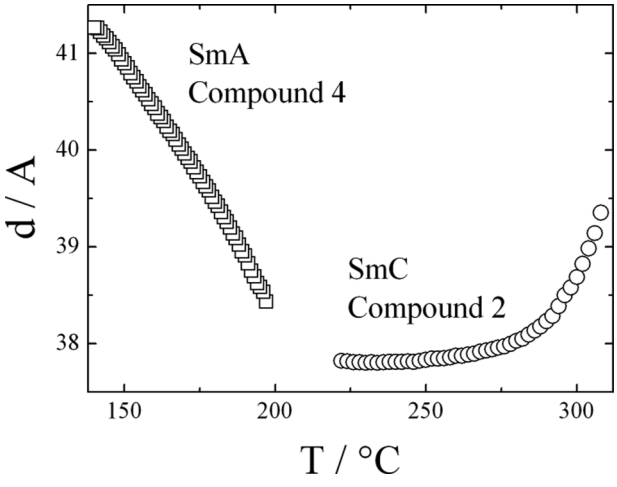

Figure 6. Temperature dependence of layer spacing in SmA phase of compound **4** and SmC phase of compound **2**.

thickness on cooling in SmC phase comes from a growing tilt angle, while the increase observed in the SmA phase can be explained by growing orientational order of molecules and changes of molecular conformations; in lower temperatures, stretched, all-trans conformations of terminal chains are more probable.

3. Conclusion

Here we have described the synthesis, current–voltage and the mesomorphic properties of a series of symmetrical rod and bent-shaped molecules in which the heptadecafluoroundecyloxy groups are linked to the core via an imino group. In order to study structure–property relationships, the lengths of the core (1–3 phenylene rings) as well as the shape of the core (rod, bent-like shape) and the kind of terminal chain (fluorinated or alkoxy chain) have been varied. The results show that both the core shape and the length of the core have a great impact on the mesomorphic behaviour. Moreover, the influence of the kind of terminal chain on the LC properties is more pronounced for the fluorinated compound compared with the alkoxy chain.

Preliminary investigations of the current–voltage characteristics for devices such as ITO/azomethine/Alq_3/Al and ITO/TiO_2/azomethine/Alq_3/Al confirmed their semiconductivity properties of the organic thin film.

4. Experimental details

4.1 Materials

All chemicals were used without any purification.

4.2 Characterisation techniques

All synthesised compounds were characterised by NMR and FTIR spectroscopy. NMR was recorded on a Bruker AC 200 MHz. Chloroform-*d* ($CDCl_3$) containing TMS as an internal standard was used as solvent. FTIR spectra of the compounds were recorded on a Perkin–Elmer paragon 500 spectrometer (wavenumber range: 400–4000 cm^{-1}; resolution: 2 cm^{-1}). Current–voltage characteristics were detected using electrometer Keithey 6517A.

The phase transitions and mesogenicity were studied by DSC and POM. DSC results were measured on a TA-DSC 2010 apparatus using sealed aluminium pans under a nitrogen atmosphere during a heating and cooling scan.

The textures of the liquid-crystalline phase were observed with a POM set-up composed of: (i) LEICA DMLM Microscope (Magnification: 2.5×, 5×, 10×, 20× and 50×) working in both transmission and reflection modes, (ii) LINKAM LTS350 (–196°C to +350°C) hot plate and LINKAM CI94 temperature controller, and (iii) JVC Numeric 3-CCD KYF75 camera (resolution: 1360 × 1024).

SAXRD studies were performed using Bruker D8 setup (CuKα line, Goebel mirror forming parallel beam, scintillation detector) equipped with heating stage DCS-350 (Anton Paar) allowing temperature

control with the precision of 0.1 K. For WAXRD studies Bruker D8 GADDS was used (CuKα line, Goebel mirrors, point beam collimator, HiStar area detector) equipped with Linkam heating stage. Experiments were done in the reflection mode for samples prepared as droplets on a heated plate.

4.3 General synthetic procedure for imines 1–5

A mixture of aldehyde (2.5 mmol) and diamine (1.0 mmol) in N,N-dimethylacetamide (DMA, 10 ml) solution, with the presence of *p*-toluenesulfonic acid (PTS) (0.06 g) was refluxed with stirring for 12 h. The reaction was conducted under an argon atmosphere. After cooling, the mixture was precipitated with 100 ml of ethanol. The crude product was washed three times with ethanol (3 × 500 ml) and two times with acetone (2 × 350 ml) to remove unreacted monomers. The compounds 1, 2, 4 and 5 soluble in dichloroethane were characterised by thin layer chromatography (TLC) on silica gel plates from E. Merck (silica gel F254) (developing solvent dichloroethane/ethyl acetate, 50/50). Then the compound was dried at 70°C under vacuum for 12 h.

4.3.1 Compound 1: bis(4-(4,4,5,5,6,6,7,7,8,8,9,9,10,10,11,11,11-heptadecafluoroundecyloxy)benzylidene)benzene-1,4-diamine

Yield: 87%. FTIR: ν_{max} in cm^{-1} 3041, 2964, 2880, 1622 (HC=N-), 1604, 1574, 1558, 1513, 1475, 1451, 1423, 1386, 1372, 1332, 1248, 1206, 1178, 1148, 1116, 1056, 1025, 984, 875, 932, 834, 737. ^{1}H NMR (200 MHz, $CDCl_3$, TMS) [ppm]: δ 8.45 (s, 2H, C**H**=N-);7.85–7.88 (m, 8H, $\mathbf{H_{Ar}}$), 7.56–7.67 (s, 4H, $\mathbf{H_{Ar}}$-CH=N-); 6.91–6.97 (m, 4H, $\mathbf{H_{Ar}}$-O); 4.07–4.14 (m, 4H, C$\mathbf{H}_2$–O); 2.31 (m, 4H, CH_2-C$\mathbf{H}_2$– CH_2-CF_2); 2.09–2.14 (m, 4H, C$\mathbf{H}_2$–CF_2). ^{13}C NMR (50 MHz, $CDCl_3$, TMS, not fully soluble) [ppm]: δ 159.51 (-**C**H=N-). Anal. Calcd. for $C_{42}H_{26}N_2F_{34}O_2$ (1236): C, 40.78; H, 2.10; N, 2.26. Found: C, 40.90; H, 2.32; N, 2.15.

4.3.2 Compound 2: bis(4-(4,4,5,5,6,6,7,7,8,8,9,9,10,10,11,11,11-heptadecafluoroundecyloxy)benzylidene)biphenyl-4,4′-diamine

Yield: 89%. FTIR: ν_{max} in cm^{-1} 3042, 2964, 2878, 1623 (HC=N-), 1607, 1592, 1573, 1511, 1487, 1450, 1423, 1401, 1327, 1333, 1310, 1250, 1204, 1170, 1148, 1135, 1117, 1055, 1025, 976, 883, 839, 738, 705, 658, 642, 530. ^{1}H NMR (200 MHz, $CDCl_3$, TMS) [ppm]: δ 8.43 (s, 2H, C**H**=N-);7.86–7.88 (m, 8H, $\mathbf{H_{Ar}}$), 7.38–7.65 (m, 8H, $\mathbf{H_{Ar}}$-CH=N-); 6.85–6.99 (m, 4H, $\mathbf{H_{Ar}}$-O); 4.02–4.13 (m, 4H, C$\mathbf{H}_2$–O); 2.31 (m, 4H, CH_2-C$\mathbf{H}_2$-CH_2-CF_2); 2.12–2.16 (m, 4H, C$\mathbf{H}_2$–CF_2). ^{13}C NMR (50 MHz, $CDCl_3$, TMS, not fully soluble) [ppm]: δ 159.61 (-**C**H=N-). Anal. Calcd. for $C_{48}H_{30}N_2F_{34}O_2$ (1312): C, 43.90; H, 2.29; N, 2.13. Found: C, 43.46; H, 2.62; N, 2.30.

4.3.3 Compound 3: bis(4-(4,4,5,5,6,6,7,7,8,8,9,9,10,10,11,11,11-heptadecafluoroundecyloxy)benzylidene)terphenyl-4,4″-diamine

Yield: 88%. FTIR: ν_{max} in cm^{-1} 3031, 2960, 2926, 2879, 1622 (HC=N-), 1607, 1591, 1572, 1510, 1485, 1451, 1423, 1400, 1372, 1333, 1312, 1250, 1204, 1168, 1148, 1116, 1055, 1026, 975, 883, 836, 818, 732, 705, 685, 658, 559, 534. ^{1}H NMR (200 MHz, $CDCl_3$, TMS) [ppm]: not soluble. Anal. Calc. for $C_{54}H_{34}N_2F_{34}O_2$ (1388): C, 46.68; H, 2.45; N, 2.02. Found: C, 46.90; H, 2.50; N, 2.10.

4.3.4 Compound 4: 4,4′-methylenebis(N-(4-(4,4,5,5,6,6,7,7,8,8,9,9,10,10,11,11,11-heptadecafluorounde cyloxy) benzylidene)benzenamine)

Yield: 89%. FTIR: ν_{max} in cm^{-1} 3025, 2956, 2918, 2880, 1626 (HC=N-), 1607, 1575, 1512, 1477, 1451, 1423, 1372, 1332, 1307, 1247, 1205, 1149, 1117, 1056, 1026, 976, 834, 738. ^{1}H NMR (200 MHz, $CDCl_3$, TMS) [ppm]: δ 8.39 (s, 2H, C**H**=N-);7.83–7.86 (m, 8H, $\mathbf{H_{Ar}}$), 7.13 (m, 8H, $\mathbf{H_{Ar}}$-CH=N-); 6.96–6.99 (m, 4H, $\mathbf{H_{Ar}}$-O); 4.01–4.13 (m, 4H, C$\mathbf{H}_2$–O); 3.95 (s, 2H, C$\mathbf{H}_2$), 2.31 (m, 4H, CH_2-C$\mathbf{H}_2$– CH_2-CF_2); 2.13–2.16 (m, 4H, C$\mathbf{H}_2$–CF_2). ^{13}C NMR (50 MHz, $CDCl_3$, TMS, not fully soluble) [ppm]: δ 161.06, 159.09 (-**C**H=N-). Anal. Calcd. for $C_{49}H_{28}N_2F_{34}O_2$ (1322): C, 44.48; H, 2.12; N, 2.12. Found: C, 44.10; H, 2.30; N, 2.23.

4.3.5 Compound 5: 4,4′-methylenebis(N-(4-(octadecyloxy)benzylidene)benzenamine

Yield: 86%. FTIR: ν_{max} in cm^{-1} 3024, 2955, 2918, 2871, 2850, 1624 (HC=N-), 1607, 1574, 1511, 1472, 1422, 1394, 1378, 1308, 1251, 1195, 1167, 1107, 1054, 1035, 1021, 977, 965, 885, 837, 817, 720. ^{1}H NMR (200 MHz, $CDCl_3$, TMS) [ppm]: δ 8.38 (s, 2H, C**H**=N-); 7.80–7.83 (m, 8H, $\mathbf{H_{Ar}}$-**O**), 7.13–7.15 (m, 4H, $\mathbf{H_{Ar}}$-CH=N-); 6.95–6.97 (m, 8H, $\mathbf{H_{Ar}}$-CH_2-$\mathbf{H_{Ar}}$), 3.99–4.03 (m, 4H, O-CH_2), 3.89–3.91 (m, 2H, C$\mathbf{H}_2$), 2.79 (m, 8H, OCH_2-(C$\mathbf{H}_2$)$_2$-), 1.26 (m, 56H, (C$\mathbf{H}_2$)$_{14}$), 0.86–89 (m, 6H, C$\mathbf{H}_3$). ^{13}C NMR (50 MHz, $CDCl_3$, TMS) [ppm]: δ 161.08, 159.33 (-**C**H=N-). Anal. Calcd. for $C_{64}H_{94}N_2O_2$ (922): C, 83.29; H, 10.19; N, 3.04. Found: C, 83.40; H, 9.98; N, 3.25.

4.4 Sol-gel technique

The samples of nanocrystalline TiO_2 were prepared by the sol-gel technique. Titanium (IV) butoxide (TBOT) was used as the titanium precursor and acetylaceton

(Acac) was applied as chelating and stabilising sol agent. The films were prepared by the sol-gel process involving three stages: (1) TBOT hydrolysis by stirring at room temperature of the system TBOT:Acac:H_2O:C_2H_5OH with molar ratios 1:4:1:27; (2) preparation of thin films by deposition and spin-coating (3000 rpm) sol on ITO substrates; and (3) gelation immediately by heating of samples at 500°C for 1 h.

4.5 Device fabrication

Current–voltage measurements were performed on ITO/compound/Alq_3/Al and ITO/TiO_2/compound/Alq_3/Al devices. Compounds were prepared on ITO–glass substrates which were cleaned in an ultra-sonic washer and organic solvents. On ITO–glass or ITO/TiO_2 substrate compounds were spread using the spin-coating method with angular speed of 880 rpm for 10 s. Tris(8-hydroxyquinolinato)aluminium is the compound with the formula $Al(C_9H_6NO)_3$, widely abbreviated as Alq_3. It is a coordination complex wherein aluminium is bonded in a bidentate manner to the conjugate base of three 8-hydroxyquinoline ligands. The chemical structure of $Al(C_9H_6NO)_3$ is presented in Figure 1.

The Alq_3 layer was prepared on the compound film surface by vacuum deposition at a pressure of 6×10^{-4} Pa and then the Al electrode was vacuum deposited at the same pressure. The area of the diodes was about 200 mm^2. Electrical measurements were performed under illuminated (about 1000 W m^{-2}) and dark conditions. A halogen lamp was used as the light source.

Acknowledgement

The authors thank Dr. Patrice Rannou for the POM experiments.

References

[1] Hird, M. *Chem. Soc. Rev.* **2007**, *36*, 2070–2095.
[2] Neubert, M.E.; Keast, S.S.; Law, C.C.; Lohman, M.C.; Bhatt, J.C. *Liq. Cryst.* **2005**, *32*, 781–795.
[3] Sakaigawa, A.; Nohira, H. *Ferroelectrics* **1993**, *148*, 71–78.
[4] Drzewinski, W.; Czuprymski, K.; Dabrowski, R.; Neubert, M. *Mol. Cryst. Liq. Cryst.* **1999**, *328*, 401–410.
[5] Stipetic, A.I.; Goodby, J.W.; Hird, M.; Raoul, Y.M.; Gleeson, H.F. *Liq. Cryst*. **2006**, *33*, 819–828.
[6] Cowling, S.J.; Hall, A.W.; Goodby, J.W.; Wang, Y.; Gleeson, H.F. *J. Mater. Chem.* **2006**, *16*, 2181–2191.
[7] Wu, S.; Lin, C. *Liq. Cryst*. **2005**, *32*, 1053–1059.
[8] Liu, H.; Nohira, H. *Liq. Cryst*. **1996**, *20*, 581–586.
[9] Takenaka, S. *J. Chem. Soc., Chem. Commun.* **1992**, 1748–1749.
[10] Bao, X.; Dix, L.R. *Mol. Cryst. Liq. Cryst.* **1996**, *281*, 291–294.
[11] Mori, A.; Uno, K.; Takeshita, H.; Takematsu, S. *Liq. Cryst*. **2005**, *32*, 107–113.
[12] Tournilhac, F.; Bilnov, L.M.; Simon, J.; Yablonsky, S.V. *Nature* **1992**, *359*, 621–623.
[13] Hird, M.; Goodby, J.W.; Gough, N.; Toyne, K.J. *J. Mater. Chem*. **2001**, *11*, 2732–2742.
[14] Glebowska, A.; Przybylski, P.; Winek, M.; Krzyczkowska, P.; Krowczynski, A.; Szydlowska, J.; Pociecha, D.; Gorecka, E. *J. Mater. Chem*. **2009**, *19*, 1359–1398.
[15] Dahn, U.; Erdelen, C.; Ringsdorf, H.; Festag, R.; Wendorff, J.H.; Heiney, P.A.; Maliszewskyj, N.C. *Liq. Cryst.* **1995**, *19*, 759–764.
[16] Terasawa, N.; Monobe, H.; Kiyohara, K.; Shimizu, Y. *Chem. Commun.* **2003**, 1678–1679.
[17] Alameddine, B.; Aebischer, O.F.; Amrein, W.; Donnio, B.; Deschenaux, R.; Guillon, D.; Savary, C.; Scanu, D.; Scheidegger, O.; Jenny, T.A. *Chem. Mater.* **2005**, *17*, 4798–4807.
[18] Kouwer, P.H.J.; Picken, S.J.; Mehl, G.H. *J. Mater. Chem.* **2007**, *17*, 4196–4203.
[19] Percec, V.; Imam, M.R.; Bera, T.K.; Balagurusamy, V.S.K.; Peterca, M.; Heiney, P.A. *Angew. Chem. Int. Ed.* **2005**, *44*, 4739–4745.
[20] Yoon, D.K.; Lee, S.R.; Kim, Y.H.; Choi, S.-M.; Jung, H.-T. *Adv. Mater*. **2006**, *18*, 509–513.
[21] Percec, V.; Glodde, M.; Johansson, G.; Balagurusamy, S.K.; Heiney, P.A. *Angew. Chem., Int. Ed.* **2003**, *42*, 4338–4342.
[22] Percec, V.; Glodde, M.; Peterca, M.; Rapp, A.; Schnell, I.; Spiess, H.W.; Bera, T.K.; Miura, Y.; Balagurusamy, S.K.; Aqad, E.; Heiney, P.A. *Chem. Eur. J.* **2006**, *12*, 6298–6314.
[23] Yamaguchi, A.; Maeda, Y.; Yokoyama, H.; Yoshizawa, A. *Chem. Mater.* **2006**, *18*, 5704–5710.
[24] Rabolt, J.F.; Russell, T.P.; Twieg, R.J. *Macromolecules* **1984**, *17*, 2786–2794.
[25] Ropers, M.H.; Stebe, M.J. *Phys. Chem. Chem. Phys.* **2001**, *3*, 4029–4036.
[26] Regev, O.; Leaver, M.S.; Zhou, R.; Puntambekar, S. *Langmuir* **2001**, *17*, 5141–5149.
[27] Rankin, S.E.; Tan, B.; Lehmler, H.; Hindman, K.P.; Knutson, B.L. *Microporous Mesoporous Mater*. **2004**, *73*, 197–202.
[28] Acimis, M.; Karaman, E.B. *J. Colloid Interface Sci.* **2006**, *300*, 1–6.
[29] Nadasi, H.; Weissflog, W.; Eremin, A.; Pelzl, G.; Diele, S.; Das, B.; Grande, S. *J. Mater. Chem.* **2002**, *12*, 1316–1324.
[30] Nastishin, Y.A.; Achard, M.F.; Nguyen, H.T.; Kleman, M. *Eur. Phys. J. E* **2003**, *12*, 581–591.
[31] Takezoe, H.; Takanishi, Y. *Jpn. J. Appl. Phys.* **2006**, *45*, 597–625.
[32] Reddy, R.A.; Tschierske, C. *J. Mater. Chem.* **2006**, *16*, 907–961.
[33] Yelamaggad, C.V.; Shashikala, I.S.; Li, Q. *Chem. Mater.* **2007**, *19*, 6561–6568.
[34] Imrie, C.T.; Henderson, P.A. *Chem. Soc. Rev.* **2007**, *36*, 2096–2124.
[35] Iwan, A.; Janeczek, H.; Kaczmarczyk, B.; Jarzabek, B.; Sobota, M.; Rannou, P. *Spectrochim. Acta Part A: Mol. Biomol. Spectrosc.* **2010**, *75*, 891–900.
[36] Iwan, A.; Janeczek, H. *Mol. Cryst. Liq. Cryst.* **2010**, *518*, 99–106.
[37] Godzwon, J.; Sienkowska, J.; Galewski, Z. *J. Mol. Str.* **2007**, *844–845*, 259–267.

[38] Marin, L.; Destri, S.; Porzio, W.; Bertini, F. *Liq. Cryst.* **2009**, *36*, 21–32.
[39] Bilgin-Eran, B.; Yorur, C.; Tschierske, C.; Prehm, M.; Baumeister, U. *J. Mater. Chem.* **2007**, *17*, 2319–2328.
[40] Iwan, A.; Janeczek, H.; Rannou, P. *Spectrochim. Acta Part A: Mol. Biomol. Spectrosc.* **2009**, *72*, 72–81.
[41] Iwan, A.; Janeczek, H.; Jarzabek, B.; Rannou, P. *Materials, Special Issue of Liquid Crystals* **2009**, *2*, 38–61.
[42] Iwan, A.; Janeczek, H.; Rannou, P.; Kwiatkowski, R. *J. Mol. Liq.* **2009**, *148*, 77–87.
[43] Yelamaggad, C.V.; Tamilenthi, V.P. *Tetrahedron* **2009**, *65*, 6403–6409.
[44] Izumi, T.; Naitou, Y.; Shimbo, Y.; Takanishi, Y.; Takezoe, H.; Watanabe, J. *J. Phys. Chem. B* **2006**, *110*, 23911–23919.
[45] Sepelj, M.; Lesac, A.; Baumeister, U.; Diele, S.; Nguyen, H.L.; Bruce, D.W. *J. Mater. Chem.* **2007**, *17*, 1154–1165.
[46] Sudhakar, S.; Narasimhaswamy, T.; Srinivasan, K.S.V. *Liq. Cryst.* **2000**, *27*, 1525–1532.
[47] Henderson, P.A.; Imrie, C.T. *Macromolecules* **2005**, *38*, 3307–3311.
[48] Kishikawa, K.; Muramatsu, N.; Kohmoto, S.; Yamaguchi, K.; Yamamoto, M. *Chem. Mater.* **2003**, *15*, 3443–3449.
[49] Cozan, V.; Gaspar, M.; Butuc, E.; Stoleriu, A. *Eur. Polym. J.* **2001**, *37*, 1–8.
[50] Iwan, A.; Bilski, P.; Janeczek, H.; Jarzabek, B.; Rannou, P.; Sikora, A.; Pociecha, D.; Kaczmarczyk, B. *J Mol. Str.* **2010**, *963*, 175–182.
[51] Iwan, A.; Janeczek, H.; Jarzabek, B.; Domanski, M.; Rannou, P. *Liq. Cryst.* **2009**, *36*, 873–883.
[52] Yoon, M.-H.; Facchetti, A.; Stern, C.E.; Marks, T.J. *J. Am. Chem. Soc.* **2006**, *128*, 5792–5801.
[53] Facchetti, A.; Mushrush, M.; Yoon, M.-H.; Hutchison, G.R.; Ratner, M.A.; Marks, T.J. *J. Am. Chem. Soc.* **2004**, *126*, 13859–13874.
[54] Pron, A.; Rannou, P. *Prog. Polym. Sci.* **2002**, *27*, 135–190.
[55] Frechet, J.M.J. *Prog. Polym. Sci.* **2005**, *30*, 844–857.
[56] Iwan, A.; Sek, D. *Prog. Polym. Sci.* **2008**, *33*, 289–345.
[57] Mitschke, U.; Bauerle, P. *J. Mater. Chem.* **2000**, *10*, 1471–1507.
[58] Elsworth, Y.; Howe, R.; Isaak, G.R.; McLeod, C.P.; New, R. *Nature* **1990**, *347*, 536–539.
[59] Sek, D.; Iwan, A.; Jarzabek, B.; Kaczmarczyk, B.; Kasperczyk, J.; Mazurak, Z.; Domanski, M.; Karon, K.; Lapkowski, M. *Macromolecules* **2008**, *41*, 6653–6663.
[60] Demus, D.; Richter, L. *Textures of Liquid Crystals*, 1st ed.; Verlag Chemie: Leipzig, 1978; pp 1–228.
[61] Gray, G.W.; Gooby, J.W. *Smectic Liquid Crystals-Textures and Structures*; Leonard Hill: Glasgow & London, 1984; pp 1–162.